Probing the Two-Metal Ion Mechanism in the Restriction Endonuclease BamHI †

5 AUTHORS, INCLUDING:

Jan Florián
Loyola University Chicago
95 PUBLICATIONS **4,140** CITATIONS

SEE PROFILE

István Simon
Hungarian Academy of Sciences
136 PUBLICATIONS **8,645** CITATIONS

SEE PROFILE

Probing the Two-Metal Ion Mechanism in the Restriction Endonuclease BamHI[†]

Letif Mones,[‡] Petr Kulhánek,[‡] Jan Florián,[§] István Simon,[‡] and Monika Fuxreiter*,[‡]

Institute of Enzymology, Biological Research Center, Hungarian Academy of Sciences, Budapest, Hungary, and Department of Chemistry, Loyola University Chicago, Chicago, Illinois 60626

Received August 13, 2007; Revised Manuscript Received September 28, 2007

ABSTRACT: The choreography of restriction endonuclease catalysis is a long-standing paradigm in molecular biology. Bivalent metal ions are required almost for all PD..D/ExK type enzymes, but the number of cofactors essential for the DNA backbone scission remained ambiguous. On the basis of crystal structures and biochemical data for various restriction enzymes, three models have been developed that assign critical roles for one, two, or three metal ions during the phosphodiester hydrolysis. To resolve this apparent controversy, we investigated the mechanism of BamHI catalysis using quantum mechanical/molecular mechanical simulation techniques and determined the activation barriers of three possible pathways that involve a Glu-113 or a neighboring water molecule as a general base or an external nucleophile that penetrated from bulk solution. The *extrinsic* mechanism was found to be the most favorable with an activation free energy of 23.4 kcal/mol, in reasonable agreement with the experimental data. On the basis of the effect of the individual metal ions on the activation barrier, metal ion A was concluded to be pivotal for the reaction, while the enzyme lacking metal ion B still has moderate efficiency. Thus, we propose that the catalytic scheme of BamHI does not involve a general base for nucleophile generation and requires one obligatory metal ion for catalysis that stabilizes the attacking nucleophile and coordinates it throughout the nucleophilic attack. Such a model may also explain the variation in the number of metal ions in the crystal structures and thus could serve as a framework for a unified catalytic scheme of type II restriction endonucleases.

Metal ion-dependent DNA cleavage is a central event in many biological processes related to the maintenance of the genome, including repair (*1−3*), combination of genetic elements, such as transposition (*4*), recombination (*5*), and homing (*6*). Although the classical mechanism for phosphoryl transfer has been developed for the 3′−5′ exonuclease of the Klenow fragment of DNA polymerase I (*7, 8*), most of the work aimed at understanding cofactor-assisted DNA degradation has been focused on restriction enzymes. Restriction endonucleases serve to protect bacteria against invading phages by recognizing and cleaving a cognate DNA sequence (*9, 10*). Metal ion(s) fulfill a dual role in this process by contributing to the formation of the tight, catalytically competent specific complex (*11*), and they also facilitate the chemical conversion (*12*). BfiI, related to the phospholipase family, is a single exception, where efficient DNA hydrolysis can be achieved in the absence of the metal cofactors (*13, 14*).

Besides the optimal Mg^{2+} ions, type II restriction endonucleases can also utilize other divalent metal ions for catalysis such as Mn^{2+}, Co^{2+}, or Fe^{2+} (*12*). Although Ca^{2+} exhibits coordination properties similar to those of Mg^{2+} in the pre-reactive state, it inhibits the reaction (*15*). Recently, quantum chemical/molecular mechanical (QM/MM)[1] calculations proposed that the coordination stress of Ca^{2+} upon conversion to the product state elevates the barrier of the nucleophilic attack step significantly (*16*), although this hypothesis has not been tested experimentally yet. The intricacies of the effects of Ca^{2+} versus Mg^{2+} and Mn^{2+} ions in restriction endonucleases hinder our understanding of these enzymes, which is further complicated by the uncertainty about how many metal ions are essential for DNA cleavage and what the exact catalytic role of each metal ion is.

Structural characterization of type II restriction endonucleases in complex with specific substrates and divalent metal ions revealed one or two metal ions at the active site at various positions, indicating diverse catalytic scenarios for these enzymes (*17*). The picture that emerges from the crystal structures of BamHI (*15*), EcoRV (*18*), and HincII (*19*) enzymes captured at different points along the reaction pathway also suggests alternative mechanisms. One can argue that these crystallographic complexes do not represent a functional state, but some were demonstrated to be fully active even in the crystal form (*15*). Apart from the main question concerning the number of metal ions required for catalysis, there is also a controversy about the mechanism

* To whom correspondence should be addressed. E-mail: monika@enzim.hu. Telephone: (36-1)-279-3138. Fax: (36-1)-466-5465.
[‡] Hungarian Academy of Sciences.
[§] Loyola University Chicago.

[1] Abbreviations: MD, molecular dynamics; EVB, empirical valence bond; FEP, free energy perturbation; QM, quantum mechanics; MM, molecular mechanics.

of nucleophile generation. On the basis of structural and biochemical data, three models have been developed that assign critical roles for one, two, or three metal ion positions at the active site.

In the one-metal ion mechanism, a single metal site is occupied at the active site, which is coordinated to the *pro-S_p* oxygen of the scissile phosphate group. Since the methylation or phosphorothioate substitution of the neghboring 3′-phosphate leads to almost complete loss of catalytic efficiency (*20*), it has been proposed that the generation of the nucleophile is achieved in a substrate-assisted manner by the phosphate group 3′ to the scissile phosphate. The metal ion stabilizes the doubly charged pentavalent intermediate generated in the nucleophilic attack step. Subsequently, a metal-bound water molecule facilitates the departure of the leaving group. This mechanism is supported by crystal structures of EcoRI (*21*) and BglII (*22*), which contain a single metal ion in the active center. Recent biochemical data on stereoselective substitutions at the EcoRI cognate sequence also support this model (*23*). On the other hand, it is quite difficult to rationalize an approximately 6 pH unit shift of the pK_a of the phosphate group from its value in water. Furthermore, the reduction of the rate upon far-away substitutions (*24*) suggests indirect electrostatic effects rather than direct involvement of the phosphate groups.

The two-metal ion mechanism has been postulated on the basis of the crystal structure for the 3′−5′ exonuclease site of the Klenow fragment of *Escherichia coli* DNA polymerase I (*7*). This model assigns a catalytic role to two metal ions that are located in parallel with the scissile bond approximately 4 Å from each other. One of the metal ions contributes to the stabilization of the nucleophile that is produced by a general base catalyst. Both metal ions are required to reduce the level of accumulation of negative charges during the attack of the OH⁻ nucleophile on the scissile phosphate group. Finally, a water molecule ligated to the second metal ion protonates the leaving group. Although the catalytic roles of both metal ions are clearly defined, their catalytic effect, i.e., their relative contributions to the reduction of the overall barrier, remains to be elucidated. Furthermore, this scenario is effective only if the two meal ions are precisely arranged to interact with the "entering" and "leaving" oxygen atoms. Metal ions at the active center of BamHI (*15*) and HincII (*19*) conform to this model, while considerable deviations are observed, for example, in EcoRV (*25*). Furthermore, the identity of the general base that is involved in generation of the nucleophile has not been identified unequivocally; it remains to be determined how Lys, Glu, and Gln located at similar positions at different restriction endonucleases can fulfill the very same role. Intriguingly, replacement of residues farther from the active site in EcoRV affected the catalysis to a greater extent than those in the proximity of the substrate (*26*). These observations might be explained by recruitment of a nucleophile from the bulk solution instead of generation of it within the active site.

The three-metal ion mechanism attempts to incorporate all three crystallographically observed metal positions into a single pathway (*18*). One metal ion stabilizes the negative charge on the nucleophile, while the *pro-R_p* oxygen of the phosphate 3′ to the scissile group helps to orient the nucleophile. This metal then triggers a conformational change
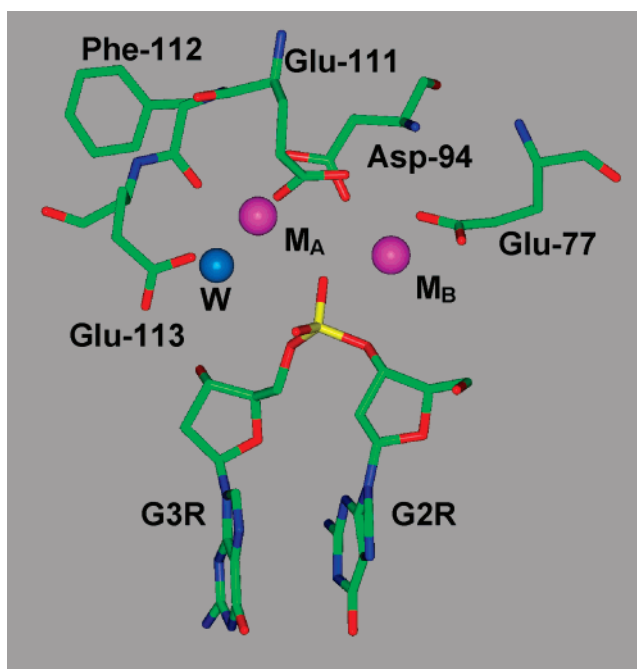

FIGURE 1: Active site of BamHI restriction endonuclease, based on the crystal structure of the pre-reactive complex in complex with a specific substrate and Ca²⁺ ions (PDB entry 2BAM). M$_A$ denotes metal ion A that coordinates the nucleophilic water molecule. M$_B$ represents metal site B that interacts with the 3′ leaving group and coordinates the water that protonates the leaving group. Glu-113 was proposed as the general base catalyst. The water that serves as the putative nucleophile is colored darker blue.

within the active site by migrating to a structurally relevant position, where it loses its coordination to the scissile phosphate and becomes ligated by two aspartates. This transition induces binding of a second metal ion, which makes a major contribution to the stabilization of the transition state, and a coordinated water molecule protonates the leaving group. Although this mechanism may account for conformational changes along the reaction pathway observed in different crystal structures of EcoRV (*27*), it faces problems with identifying the general base and explaining why the catalytically relevant positions are not occupied at the same time.

In this work, we have investigated the catalytic mechanism of BamHI endonuclease using the empirical valence bond (EVB) approach in combination with molecular dynamics (MD) and free energy perturbation (FEP) techniques. BamHI is a structurally well characterized member of the PD..D/ExK family that recognizes the palindromic GGATCC sequence and cleaves between the two guanines (*15, 28, 29*). The crystal structures of pre- and postreactive complexes of BamHI (*15*) are in accord with a two-metal ion mechanism. In addition to two Mg²⁺ ions, the active site of BamHI contains three negatively charged residues, where Glu-113 replaces the lysine that is generally present in other enzymes and was proposed to play role as a general base (*15*) (Figure 1). We have studied three possible pathways, where the nucleophile is generated via a general base mechanism by Glu-113 (i), a proton abstraction by a nearby water molecule (ii), or penetration of the OH⁻ from bulk solution (iii), and identified *extrinsic* mechanism iii as the preferred pathway.

To quantify the individual contributions of the metal ions to the overall catalytic effect, we examined how the absence

of one of the two crystallographic Mg^{2+} ions and positional restraint of the remaining ion alter the free energy barriers for mechanisms i and iii and if these barriers can be lowered by the metal repositioning. These calculations revealed the greatly different catalytic importance of the two metal ions: metal A assisting the nucleophile generation is critical for BamHI catalysis, whereas metal ion B is auxiliary and contributes to a lesser extent. These conclusions are also supported by previous MD (30) calculations and metal competition experiments (A. Pingoud, private communication). The emerging model could provide a general framework for other PD..D/ExK type enzymes.

MATERIALS AND METHODS

Calculations of the Activation Barriers. To compute the activation free energy of different mechanisms, the EVB method (31) was applied in combination with the FEP technique. The robustness of the method in modeling chemical reactions in solution and in an enzymatic environment was demonstrated for several enzymes and is illustrated by the good agreement between the computed and experimental activation barriers (32). The method has been described in the literature in detail (33, 34); therefore, only the main features are outlined here.

The EVB model treats the reaction as a transition between different resonance states that are described by a molecular mechanical model. The energy of each diagonal element of the Hamiltonian represents the energy of the resonance states:

$$E_i = H_{ii} = \sum_j \Delta M_j^{(i)}[b_j^{(i)}] + \frac{1}{2}\sum_l k_{l,b}^{(i)}[b_l^{(i)} - b_{l,0}^{(i)}]^2 +$$
$$\frac{1}{2}\sum_m \gamma_{m,\theta}^{(i)} k_{m,\theta}^{(i)}[\theta_m^{(i)} - \theta_{m,0}^{(i)}]^2 +$$
$$\sum_n \gamma_{n,\phi}^{(i)} k_{n,\phi}^{(i)}\{1 + \cos[n_n^{(i)}\phi_n^{(i)} - \delta_n^{(i)}]\} +$$
$$U_{nb,rr}^{(i)} + \alpha^{(i)} + U_{nb,rs}^{(i)} + U_s \quad (1)$$

where $\Delta M_j^{(i)}$ is the Morse potential of the jth affected bond (which is formed or broken during the reaction) in the ith resonance state and the second term is a harmonic potential for other bonds. The following two terms are the angle bending and torsion terms relative to their minima in the ith resonance state where $\gamma_{m,\theta}^{(i)}$ and $\gamma_{n,\phi}^{(i)}$ are the coupling terms between angles/torsion angles constituted by those bonds that are affected by the reaction (form or break). $U_{nb,rr}^{(i)}$ and $U_{nb,rs}^{(i)}$ denote the nonbonded interactions (van der Waals and electrostatic) between the reactive groups and between the reactive and surrounding protein and solvent groups, respectively. U_s is the internal energy of the protein/solvent system. $\alpha^{(i)}$ is the gas-phase energy of the ith resonance state, when all fragments are at infinite separation. The off-diagonal elements of the Hamiltonian are usually represented by an exponential function:

$$H_{ij} = A_{ij} \exp\{-\mu r_{ab}\} \quad (2)$$

where r_{ab} is the representative distance between two atoms whose bonding is changed from the ith to jth resonance state, whereas A_{ij} and μ are parameters. The values of the $\alpha^{(i)}$, A_{ij}, and μ parameters are calibrated in a postprocessing process

to the experimental data of the reference reaction in water. The gas-phase shift is set to the free energy of the reaction, while the off-diagonal elements (A and μ) are adjusted against the activation free energy.

The combination of the diabatic energies of the resonance states via the diagonalization of the EVB Hamiltonian gives the true (quantum mechanical) ground state energy (E_g). The EVB treatment is combined with a FEP protocol by driving the system along a mapping potential constructed as

$$E_m = \sum_{i=0}^{N} \lambda_i^m E_i \quad (3)$$

where for each m the sum of λ_i^m values is 1. For each i, λ_i^m is changing between 0 and 1 in a series of $N + 1$ steps (FEP windows) as the reaction proceeds if two resonance states are considered. The free energy upon changing the mapping potential between two consecutive steps is given by

$$\delta G_{m \to m+1} = -\beta^{-1} \ln\{\langle \exp[-(E_{m+1} - E_m)\beta]\rangle_m\} \quad (4)$$

where the broken brackets denote averaging over trajectories on mapping potential E_m. $\beta = 1/k_B T$, where k_B is the Boltzmann constant. If the perturbation is infinitely small upon going from E_m to E_{m+1}, then such a FEP procedure will provide exact results. The sum of the free energy changes provides the total free energy of the reaction. The activation free energy must be evaluated in reference to the ground state potential by using the umbrella sampling formula:

$$\Delta g(X') = \Delta G_m - \beta^{-1} \ln\langle \delta(X - X')$$
$$\exp\{-\beta[E_g(X) - E_m(X)]\}\rangle_{E_m} \quad (5)$$

where E_m is a mapping potential that brings X general reaction coordinate closest to X′ representing the transition state.

Models. The initial structure was derived from the crystal structure of BamHI in complex with a specific dodecamer DNA and inhibitor Ca^{2+} ions (PDB entry 2BAM) (15). The Ca^{2+} ions were replaced with catalytically active Mg^{2+} ions, and the structure was completed with hydrogens using the Amber program package (35). The crystal structure has been immersed in a sphere of TIP3P water molecules with a 30 Å radius centered on the phosphorus atom of the scissile phosphate. Overall, electroneutrality of each model was ensured by neutralizing those Glu and Asp side chains that are far from the catalytic center but not located on the protein surface. For the reference reaction in water, instead of the Mg^{2+} ions two Na^+ counterions were included to neutralize the system. Four models were constructed: (I) both crystallographic A and B sites occupied, (II) a single metal ion at site A, (III) a single metal ion at site B, and (IV) a single metal ion located at site A′ obtained by optimization of site A (32).

The structure with two Mg^{2+} ions (model I) has been relaxed using the following protocol. The system was gradually heated to 298 K in a 500 ps simulation using a 0.01 fs time step in the first 1 ps, then a 0.1 fs time step in the next 10 ps, and finally a 0.5 fs time step from 11 to 500 ps. A restraint of 100 kcal mol^{-1} $Å^{-2}$ has been applied on the Mg^{2+} ions to keep them close to their crystallographic
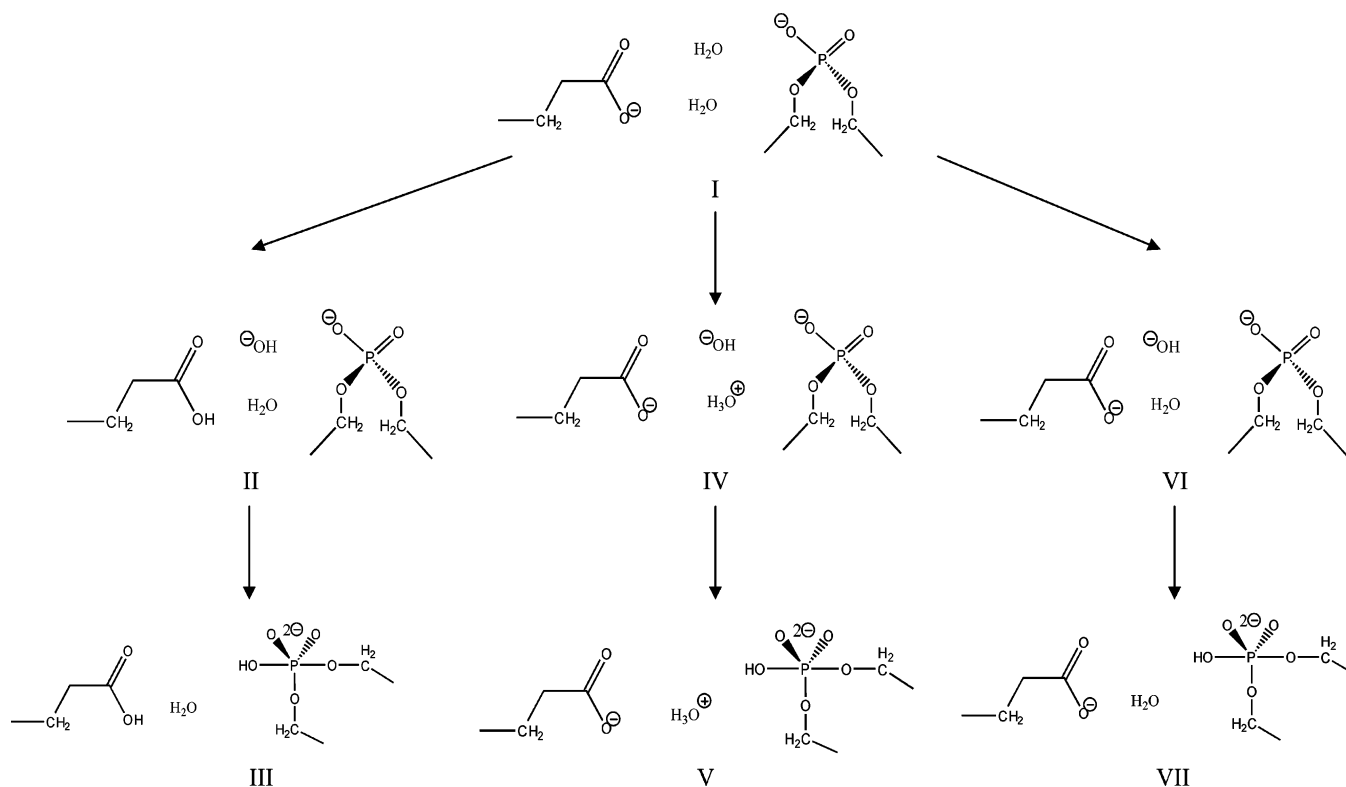
FIGURE 2: Resonance structures of the three mechanisms considered for BamHI catalysis. I represents the pre-reactive state. The I → II → III pathway is the general base mechanism involving Glu-113. The I → IV → V pathway represents the nucleophile generation by a neighboring water molecule. The I → VI → VII pathway is the *extrinsic* mechanism, when the nucleophile is recruited from bulk solvent.

positions, which was gradually decreased to 5 kcal mol^{-1} Å^{-2} in the last 200 ps. The metal ions were not constrained to another atom(s), rather a harmonic constraint being applied to tether them to their crystallographic *xyz* coordinates, which made up the starting point of our simulations. The structures with a single metal ion at site A (model II) or site B (model III) have been relaxed similarly except that the restraint on the ions was gradually decreased from 100 to 15 kcal mol^{-1} Å^{-2} in the last 200 ps. As we wanted to probe the catalytic importance of the crystallographically observed positions, we kept a 5 kcal mol^{-1} Å^{-2} constraint on the metal ions during the simulation of the chemical steps. The rationale behind these constraints was to evaluate the energetics of the catalyzed reaction in the presence of metal ions at their crystallographically observed sites and thereby provide a direct probe of the Steitz model (*8*). When the constraints were fully relaxed, metal ion A remained very close to its crystallographic position, leaving the energetics of the reaction almost unaffected (see also Table 2). Metal ion B tends to move away from its crystallographically observed site by ~2 Å, but this shift does not have a significant impact on the activation barrier [note that the complete removal of metal ion B increases the activation energy by only 6.5 kcal/ mol (see Table 2)]. Since our force field is capable of reproducing correct metal−ligand coordination distances in various systems (*36*), the movement of metal ion B should reflect a real dynamics of the model, rather than the artifact of the force field. The structure with a single metal ion located at A′ (model IV) was gradually heated to 298 K in a 250 ps simulation using a 0.01 fs time step in the first 1 ps, then a 0.1 fs time step in the next 10 ps, and a 0.5 fs time step from 11 to 250 ps. The restraint on the metal ion

was gradually released from 50 kcal mol^{-1} Å^{-2}, and in the last 100 ps, an unconstrained simulation was applied.

Resonance Structures. The reactive region included the scissile phosphate, the nucleophilic water, and the potential general base: the carboxyl group of Glu-113, a neighboring water molecule that is hydrogen bonded to the putative nucleophile. For the reference reaction in water, a dimethyl phosphate, a propionic acid, and two water molecules were considered. Figure 2 summarizes the resonance structures corresponding to three different pathways: (i) Glu-113 serves as a general base, (ii) the neighboring water abstracts the proton, and (iii) the OH$^-$ comes from bulk solution.

Computational Details. All calculations were performed within the framework of the Q program (*37*). Simulation of each reaction step was achieved by a 125 ps long FEP/MD calculation using 50 windows. The time step of 0.5 fs was applied, and all protein atoms were tethered to their crystallographic positions by a harmonic force of 5 kcal mol^{-1} Å^{-2}. For the outer water shell, a 20 kcal mol^{-1} rad^{-2} polarization constraint was applied. The protein was represented by an Amber '95 force field (*38*). To avoid artificially short contacts between the nucleophile and the nearby metal ion and also to reproduce the distance between the metal ion and the phosphate oxygens observed in crystal structures, we increased the van der Waals radius of the Mg^{2+} to 1.3 Å, while that of the negatively charged oxygens was modified to 1.9 Å as previously proposed (*36*). van der Waals radii of the O and H atoms in the OH$^-$ group were 1.9 and 0.1 Å, respectively, and their partial charges were −1.0 and 0.0, respectively.

Simulation of the Proton Transfer Step. Three mechanisms of nucleophile generation have been considered. Since these

Table 1: Reaction (ΔG_0) and Activation ($\Delta g^{\ddagger}$) Free Energies of the Phosphodiester Hydrolysis in Water and in Protein with the EVB Parameters Calibrated for the Reference Reactions[a]

reaction	water					protein			
	$\alpha^{(i)}$	H_{ij}	ΔG_0	$\Delta g^{\ddagger}$	$\Delta G^{\ddagger}$	ΔG_0	$\Delta g^{\ddagger}$	$\Delta G^{\ddagger}$	$\Delta\Delta G^{\ddagger}$
			General Base Catalysis by Glu-113						
I → II	81.2	29.1	15.7[b]	18.3[b]		−1.2	4.4		−16.9
II → III	430.7	49.9	31[c]	33[c]		30.5	30.8		−2.2
total					48.7			29.6	−19.1
			Proton Transfer to a Neighboring Water						
I → IV	205.8	86.7	21.7[d]	25.1[d]		23.6	25.4		1.9
IV → V	433.9	53.2	31	33		50.4	52.2		19.2
total					54.7			75.8	21.1
			Extrinsic Mechanism						
I → VI (solvent)[c]	−30.1	0.0	−101.0[e]	−		−114.6	−		−13.6
I → VI			11.8			−1.8			−13.6
VI → VII	439	47.9	31	33		23.6	25.2		−7.8
total					44.8			23.4	−21.4

[a] $\alpha^{(i)}$ denotes the gas-phase shift of the given resonance state (eq 1, Figure 2), and H_{ij} represents the off-diagonal term between resonance states i and j (eq 2). $\Delta G_{w}^{\ddagger}$ and $\Delta G_{p}^{\ddagger}$ are the overall activation barriers of the reaction in water and protein, respectively. The catalytic effect is defined as $\Delta\Delta G^{\ddagger} = \Delta G_{p}^{\ddagger} - \Delta G_{w}^{\ddagger}$. For the nucleophile generation step, a difference between the ΔG_0 values is considered, and for the nucleophilic attack, the difference between the $\Delta g^{\ddagger}$ values is considered (see eq 12). All values are given in kilocalories per mole. Roman numerals correspond to resonance structures displayed in Figure 2. [b] ΔG_0 and $\Delta g^{\ddagger}$ values are calibrated against the experimental values given in refs *39* and *40*. [c] ΔG_0 is calibrated against the result of high-level ab initio calculations (*45*), and $\Delta g^{\ddagger}$ values are calibrated against experimental data (*46*). [d] ΔG_0 and $\Delta g^{\ddagger}$ values are calibrated against the experimental values given in ref *39*. [e] ΔG_0 is calibrated against the solvation free energy difference of water and hydroxide in bulk solvent obtained by the Iterative Langevin Dipole method.

involve microscopic evaluations of proton transfer in water as well as in the protein site, no assumption was made about the pK_a values of the participating residues in the protein environment. In particular, for the general base mechanism with Glu-113, we started the EVB calculation with deprotonated carboxylate and determined the ΔpK_a between the proton donor (H$_2$O) and acceptor (Glu) from the calculated reaction free energies for the proton transfer in water and in the protein (see eqs 6−9 below). For the calibration of the proton transfer reaction in aqueous solution, we used experimental pK_a values of 15.7 and 4.3 for water and Glu, respectively. Since in case of the *extrinsic* mechanism the proton from the putative nucleophile is transferred to bulk, we simulated this process by annihilating one of the protons of the nucleophilic water molecule. This was realized by turning off all van der Waals and Coulombic parameters of the given proton (in H$_2$O, r_H = 0.1 Å and q_H = 0.417; parameters of the OH$^-$ group are given in Computational Details) in a free energy perturbation procedure, using 50 windows with a total simulation time of 125 ps, with a time step of 0.5 fs. The calibration of this reaction is described below (see also the footnotes of Table 1).

RESULTS

Energetics of the Reference Reactions in Water. The free energy of the proton transfer processes is given by the difference between the pK_a values of the donor and acceptor groups:

$$\Delta G_{PT}(AH + B^- \rightarrow A^- + BH) =$$
$$2.303RT[pK_a(AH) - pK_a(HB)] \quad (6)$$

We determined ΔG_{PT} values in the protein active site using the EVB method calibrated on ΔG_{PT} obtained from the experimental pK_a difference in aqueous solution. In particular, ΔG_{PT} for the transfer of a proton from water to glutamate costs 15.7 kcal/mol in bulk solvent, while that between two

water molecules is less favorable. The calibrated EVB parameters and the corresponding free energy values are listed in Table 1. The activation free energy of the general base mechanisms by glutamate and water was calibrated against experimental data (*39*, *40*) (and see also the footnotes of Table 1).

The pK_a of the water nucleophile can be estimated on the basis of the free energy differences between converting a water molecule to hydroxide in water (w) and within the active site of the enzyme (p):

$$\Delta\Delta G_{PT}^{w\rightarrow p} = \Delta G[(H_2O)^p \rightarrow (H_2O)^w] +$$
$$\Delta G[(OH^-)^w \rightarrow (OH^-)^p] = \Delta G[(H_2O \rightarrow OH^-)^p] -$$
$$\Delta G[(H_2O \rightarrow OH^-)^w] \quad (7)$$

Equation 7 was used to compute the difference in the solvation free energy of a water molecule and the hydroxide ion in the enzymatic environment of BamHI, $\Delta G[(H_2O) \rightarrow (OH)^-]^p$, as compared to water (Table 1, I → VI, first line). The standard free energy used for calibrating the creation of a hydroxide in the bulk solution, $\Delta G[(H_2O) \rightarrow (OH)^-]^w$, was determined computationally by the Iterative Langevin Dipole method to be −101 kcal/mol, in reasonable agreement with experimental data [−103.6 kcal/mol (*41*)] and with previous computational results (*42*).

On the basis of the $\Delta\Delta G_{PT}^{w\rightarrow p}$ obtained with eq 7, the pK_a of the water nucleophile can be evaluated as

$$pK_a^p(H_2O) = pK_a^w(H_2O) + \frac{\Delta\Delta G_{PT}^{w\rightarrow p}}{2.3RT} \quad (8)$$

Its value can be derived as 5.7 in the presence of two metal ions. Using this pK_a, the free energy cost of hydroxide ion formation in the protein by the *extrinsic* mechanism can be computed as (*43*, *44*)

$$\Delta G_{PT}(OH_{ext}^-) = 2.303RT[pK_a^p(H_2O) - pH] \quad (9)$$

This free energy for hydroxide ion formation via the *extrinsic* mechanism amounts to 11.8 kcal/mol (Table 1).

The energetics of the nucleophilic attack step have been calibrated using the free energy of 31 kcal/mol of transforming a phosphodiester to a dianionic pentavalent intermediate in aqueous solution at pH 15.5 (1 M OH$^-$) based on high-level ab initio calculations (*45*), while the corresponding activation free energy ($\Delta g^\ddagger = 33$ kcal/mol) was derived from Guthrie's thermochemical data (*46*), which coincided with ab initio results (*45*). The similarity of the energy of the pentavalent intermediate to that of the transition state indicates that the reaction is "semi-concerted"; i.e., entering of the nucleophile and the departure of the leaving group occur almost simultaneously.

The overall barrier of the reaction is given by

$$\Delta G^\ddagger = \Delta G_{PT} + \Delta g^\ddagger_{NA} \quad (10)$$

where ΔG_{PT} is the free energy of proton transfer and $\Delta g^\ddagger_{NA}$ is the activation free energy of the nucleophilic attack. With regard to the overall barrier of the phosphodiester hydrolysis in water, the general base catalysis by glutamate is more favorable by 6 kcal/mol than the mechanism, which recruits another water molecule for proton transfer. The most favorable process employs a OH$^-$ nucleophile generated at pH 7 with an overall barrier of 45 kcal/mol. This value is in reasonable agreement with other experimental and theoretical estimates of the barrier of neutral phosphodiester hydrolysis (see the discussion in ref *4* and references therein). We have to emphasize that here we considered a stepwise process and depending on the degree of concertedness of the two reaction steps the overall barrier can be lowered by 5−7 kcal/mol.

Defining the Catalytic Effect of the Enzyme. The overall barrier of the enzyme is composed of the free energy of proton transfer in the enzyme and free energy barrier of the nucleophilic attack as

$$(\Delta G^\ddagger)^p = (\Delta G_{PT})^p + (\Delta g^\ddagger_{NA})^p = (\Delta G_{PT})^w +$$
$$(\Delta\Delta G_{PT})^{w\rightarrow p} + (\Delta g^\ddagger_{NA})^w + (\Delta\Delta g^\ddagger_{NA})^{w\rightarrow p} \quad (11)$$

where $(\Delta\Delta G_{PT})^{w\rightarrow p}$ and $(\Delta\Delta g^\ddagger_{NA})^{w\rightarrow p}$ terms are the differences between the free energy of proton transfer and activation free energy in water and enzyme, respectively. The first-order rate constant for the first strand cleavage by BamHI is 0.46 s^{-1}, which gives a $(\Delta G^\ddagger)^p$ of 17.9 kcal/mol (*47*). The catalytic effect of the enzyme is defined as

$$(\Delta\Delta G^\ddagger)^{w\rightarrow p} = (\Delta G^\ddagger)^p - (\Delta G^\ddagger)^w = (\Delta\Delta G_{PT})^{w\rightarrow p} +$$
$$(\Delta\Delta g^\ddagger_{NA})^{w\rightarrow p} \quad (12)$$

that is estimated to be 26.9−36.8 kcal/mol depending on the mechanism of nucleophile generation.

Energetics of the Reaction in the BamHI Active Site. Free energies and activation barriers of the three pathways are summarized in Table 1. Both the general base and *extrinsic* mechanisms are favored by the enzyme, while the proton transfer to a neighboring water is destabilized. This is primarily due to the repulsion between the hydroxonium ion and the proximal metal ion cofactor that is not shielded

completely by the generated hydroxide. Furthermore, at the end of the proton transfer process, metal ion A becomes bound to Glu-113. This coordination has to be broken during the nucleophilic attack step, while the metal ion shifts by almost ∼2 Å to ligate the nonbridging oxygens of the scissile phosphate group. Meanwhile, the H$_3$O$^+$ ion is repelled from the active site, which contributes to a further increase in the activation barrier.

Both reaction steps of the general base and the *extrinsic* mechanisms are energetically more favorable in the active site of BamHI than in water. Involving Glu-113 as a general base exerts a greater stabilization on the generation of the nucleophile as compared to recruiting an external nucleophile from bulk solvent. The resulting glutamic acid, however, strongly binds the OH$^-$ group that overstabilizes the nucleophile and leads to a higher barrier for the nucleophilic attack step. Considering the overall barrier, the *extrinsic* mechanism is more favorable than the general base catalysis with a total activation energy of 23.4 kcal/mol. The computed total activation free energy is in reasonable agreement with the experimental value, and their 5 kcal/mol difference is mostly due the concertedness of the reaction. This effect was not taken into account in our calculations and, along with limited simulation time and metal constraints, might contribute to the overestimation of the activation barrier.

Three possible mechanisms of the nucleophile generation step have also been studied previously with the semimicroscopic version of the Protein Dipoles/Langevin Dipoles method (PDLD/S) (*48*). These calculations excluded the role of the neighboring phosphate as the general base and concluded, in accord with this work, that the *extrinsic* mechanism in the presence of negatively charged Glu-113 is the most favorable pathway. The two studies yielded close pK_a values for the water nucleophile: 5.7 by the EVB/FEP technique and 5.3 by the PDLD/S method. The pK_a values of Glu-113 in the two studies exhibited opposite trends: protonation was found to be more favorable than that in water by EVB/FEP ($pK_a = 6.7$), while it was less favorable in the PDLD/S study ($pK_a = 2.9$). This discrepancy is due to the difference in the force field used (AMBER vs ENZYMIX) as well as the treatment of the neighboring phosphate groups, which were kept neutral in the PDLD/S study but were considered charged in this work.

In the case of the *extrinsic* mechanism, the nucleophile is bound to metal ion A. One might wonder if the barrier of the nucleophilic attack by a hydroxide coordinated to the metal ion is not prohibitive. This is equivalent to the nucleophile trapping problem; i.e., overstabilization of the nucleophile can lead to an excessive increase in the barrier of the nucleophilic attack step. As demonstrated by the $\Delta g^\ddagger_{NA}$ value presented in Table 1, this step is optimized to a smaller extent than the generation of the nucleophile, yet it is still more favorable in the enzyme by 7.8 kcal/mol than the corresponding reference reaction in water [note the $(\Delta\Delta g^\ddagger_{NA})^{w\rightarrow p}$ is negative]. This catalysis can be explained easily by the inspection of the transition state structure displayed in Figure 3. During the nucleophilic attack step, the hydroxide remains bound to metal ion A at the transition state, while it approaches the phosphorus. Such a scenario was predicted by a recent molecular dynamics studies that explored the stability of the metal ion sites at the active site of BamHI (*30*).
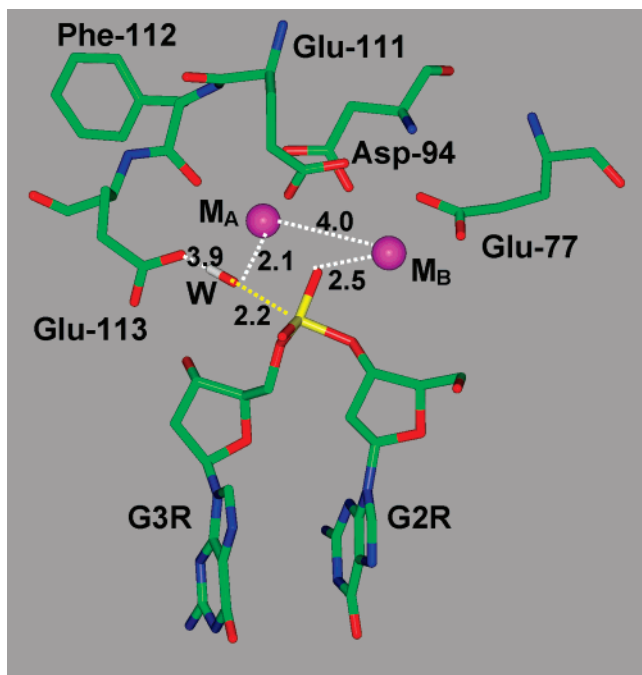
FIGURE 3: Transition state structure of the nucleophilic attack in the presence of two metal ions at the active site of BamHI as determined by the EVB/FEP calculations. Coordination distances are given in angstroms.

FIGURE 4: Transition state structure of the nucleophilic attack in the presence of a single metal ion at site A′ of BamHI as determined by the EVB/FEP calculations. In the absence of metal ion B, Glu-77 points away from the active site. Coordination distances are given in angstroms.

Role of Metal Ions. The arrangement of the metal ions at the active site of BamHI conforms to the classical two-metal ion mechanism of phosphoryl transfer. The significantly larger stabilization of the nucleophile generation as compared to the subsequent step and the distinguished role of metal ion A in this process might indicate that the catalytic importance of the two metal ions, i.e., their contribution to the overall catalytic effect, is different.

To clarify the role of the metal ions and quantify their catalytic importance, we have determined the overall barrier of the phosphoryl transfer reaction in the presence of individual metal ions bound at positions A, A′ [shifted by 0.9 Å from the crystallographic A position (*30*)], and B. To this end, we constructed hypothetical enzymes with a single metal ion at position A or B at the active site and constrained them to their initial positions during the reaction. Position A′ was created after the nucleophile generation step, and its role was probed only during the nucleophilic attack. To investigate whether the removal of one metal ion may change the mechanism realized in the presence of two metal ions, two pathways were considered for activation energy calculations: the general base mechanism by Glu-113 and the *extrinsic* mechanism. The third scenario with proton transfer between two neighboring water molecules was excluded due to its unfavorable energetics in the enzymatic environment.

The respective free energies of the proton transfer reaction and the activation free energies of the nucleophilic attack are summarized in Table 2. The overall barrier of the general base mechanism is affected by the removal of one metal ion to a lesser extent than that of the *extrinsic* mechanism. Nevertheless, the scheme involving an external nucleophile still provides the most favorable pathway when site A or site A′ is solely occupied (Figure 4). Overall barriers computed in the presence of a single metal ion occupying either site A or B demonstrate that the catalytic importance
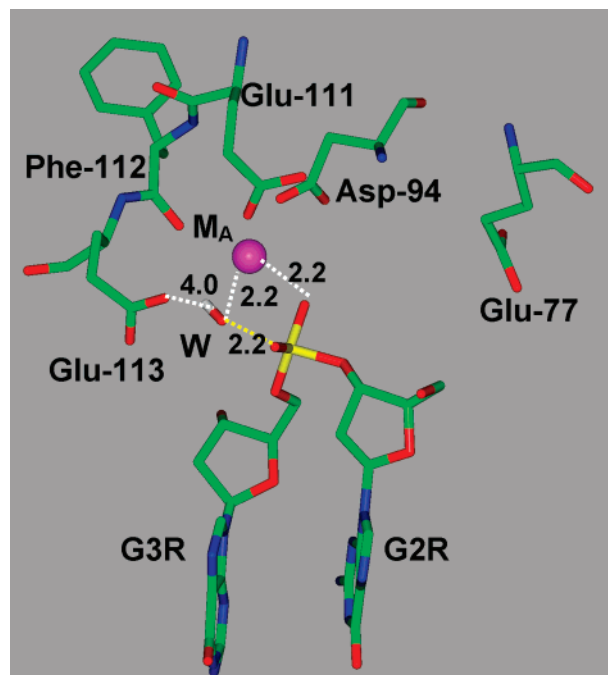
(effect) of the two metal sites is different. In the presence of the single metal ion A, the activation free energy is increased by 6.5 kcal/mol. In contrast, when only metal ion site B is occupied, the proton transfer process becomes rate-limiting and the reaction becomes less favorable than in water. This result is associated with the difficulties of the nucleophile stabilization in the absence of the coordinating metal ion A. The large barrier obtained with our calculations is due to electrostatic repulsion from the nearby negatively charged residues (Asp-94, Glu-111, Glu-113, and the scissile phosphate). These contributions are likely overestimated because the simulations do not allow ionizable residues to change their protonation state and are too short for Na^+ ions to diffuse into the active site to stabilize the negative charges in the absence of Mg^{2+}. Unfortunately, more realistic models that could take these effects into account are too demanding to be implemented in the framework of current state of the art simulations. Nevertheless, we believe that the predicted abolition of the catalytic effect would also be realized using more sophisticated calculations.

The total activation energy in the presence of a single metal ion at the optimized site A′ exceeds the barrier obtained in the presence of two metal ions by only 6.1 kcal/mol. On the basis of previous ground state MD simulations (*30*), we expected that a single metal ion at site M, located approximately halfway between the crystallographically observed A and B sites (*30*), will provide the largest contribution to catalysis. Thus, we attempted to move the metal ion from A′ to M during the nucleophilic attack. Although at site M the metal ion coordinates both nonbridging oxygens of the phosphate group, its coordination sphere becomes severely distorted; thus, it increases the activation barrier of the nucleophilic attack by more than 10 kcal/mol, depending on the strength of the constraint (not shown in Table 2).

Table 2: Reaction (ΔG_0) and Activation ($\Delta g^{\ddagger}$) Free Energies at the Active Site of BamHI with a Single Metal Ion at Crystallographically Observed Site A, Site B, or the Optimized Site A$'^a$

reaction	A				B				A$'$			
	ΔG_0	$\Delta g^{\ddagger}$	$\Delta G_p{}^{\ddagger}$	$\Delta\Delta G^{\ddagger}$	ΔG_0	$\Delta g^{\ddagger}$	$\Delta G_p{}^{\ddagger}$	$\Delta\Delta G^{\ddagger}$	ΔG_0	$\Delta g^{\ddagger}$	$\Delta G_p{}^{\ddagger}$	$\Delta\Delta G^{\ddagger}$
General Base Catalysis by Glu-113												
I → II	0.8	7.3		−14.9	31.6	31.6		15.9	−2.5	5.5		−18.2
II → III	33.8	33.8		−0.2	48.2	50.2		17.2	34.5	34.5		1.5
total			34.6	−15.1			81.8	33.1			32	−16.4
Extrinsic Mechanism												
I → VI (solvent)^b	−112.1	−		−11.1	−54.1	−		46.9	−112.1	−		−11.1
I → VI	0.7			−11.1	58.7			46.9	0.7			−11.1
VI → VII	28.9	29.2		−3.8	101.6	104.3		71.3	28.8	28.8		−4.2
total			29.9	−14.9			163	118.2			29.5	−15.3

^{a} The catalytic effect is defined as $\Delta\Delta G^{\ddagger} = \Delta G_p{}^{\ddagger} - \Delta G_w{}^{\ddagger}$. For the nucleophile generation step, a difference between the ΔG_0 values is considered, and for the nucleophilic attack, the difference between the $\Delta g^{\ddagger}$ values is considered (see eq 12; for corresponding values in water, see Table 1). The meaning of symbols is the same as in Table 1. ^{b} Solvation free energy of the OH$^-$ group.

DISCUSSION

With the exception of BfiI (*13*), all restriction endonucleases require Mg^{2+} ions for catalysis, but the variable number of the metal ion sites located in the crystal structures of restriction endonuclease ternary complexes has made the exact number of catalytic ions subject of a long-standing debate (*17*). Three catalytic models have been developed to account for different numbers of metal ions and positions in the course of phosphoryl transfer that involves one, two, or three metal ions at the active site. Although all models agree that the proximity of the metal ion to the putative nucleophile facilitates the nucleophile preparation step by decreasing the pK_a of this nucleophile, there has been a long pursuit of identification of residues that can serve as a general base catalyst. Although mutations reducing the catalytic rate suggested some candidates, the general base could not be unequivocally localized.

Our earlier computational analysis of the energetics of the nucleophile preparation step has indicated that recruiting OH$^-$ from bulk solvent (*extrinsic* mechanism) is more favorable than preparing it with the assistance of a general base at the active site, either by Glu or by the 3$'$-phosphate group (*48*). This study, however, did not consider the barrier of the subsequent reaction step, thus leaving open an option for either mechanism to become eliminated due to the nucleophile trapping.

This comparison of the activation free energies of the three catalytic models in BamHI confirms that the mechanism involving an external nucleophile, i.e., moving a proton to bulk solvent, is the most favorable. A barrier of 23 kcal/mol calculated for the *extrinsic* mechanism in the presence of metal ions constrained to their crystallographic positions is in reasonable agreement with the activation free energy derived from experimental values for a stepwise process.

BamHI exerts a greater stabilization on the nucleophile preparation than on the nucleophilic attack step due to the coordination of the OH$^-$ group to metal A. This coordination persists throughout the nucleophilic attack step, but the catalytic effect of the enzyme on this step is smaller than on the nucleophile preparation step. This result contradicts earlier suggestions that the energetics of the nucleophilic attack is optimized more by evolution than the nucleophile generation step (*17*). The *extrinsic* mechanism, i.e., that the putative nucleophile water is not deprotonated by an active site residue, may resolve the ambiguity in the identity of

the general base. However, it remains to be explained why the catalytic effect of a distant Lys-173 in EcoRV is comparable to that of Lys-92 lying in the active site of the enzyme (*26*) or how phosphates 4 bp from the scissile phosphate can contribute to catalysis (*24*). The proposed mechanism lacking a general base catalyst represents a promising lead in this respect because it requires the buildup of a larger negative charge, and the stability of this negative charge may be sensitive to longe-range electrostatic effects. The *extrinsic* mechanism is also in accord with recent biochemical and structural data on EcoRI (*23*) and does not contradict the observations with HincII (*19*) and EcoRV (*18*).

The BamHI crystal structure contains two metal ions at the active site that are perfectly arranged for the classical two-metal ion mechanism. By calculating activation free energies for structural variants of BamHI which contained a single constrained metal, we dissected the overall catalytic effect into contributions of each metal site. This free energy decomposition has an advantage over decomposition schemes based on evaluating force field contributions within a single FEP calculation (*49*) in that it takes into account structural effects, but it may be associated with significant nonadditivity effects (*50*). Nevertheless, our constraint-based approach provides well-defined catalytic contributions and can be generalized to other enzymes with multiple metal sites, including those in which the actual number of occupied sites is uncertain (*51*).

The catalytic importance of the two metal ions differs significantly: the absence of metal B resulted in moderate changes in the total activation barrier, whereas the removal of metal from site A abolished the catalytic effect of the enzyme. Metal A is critical for stabilizing the nucleophile and also helps the nucleophilic attack by coordinating the nucleophile throughout the formation of the pentavalent intermediate. In the absence of metal ion A, nucleophile generation becomes the rate-limiting step of the reaction.

On the basis of moderate changes in the barrier upon removal of metal ion B as well as our previous data on the stability of the metal ion sites, we suggest that only one metal ion is essential for BamHI catalysis. It is, however, possible that the catalytic importance of metal B would increase when the last reaction step, P−O bond breaking, is fully taken into account. In this study, we did not evaluate explicitly this reaction step but instead assumed that the structure of the

transition state for the nucleophilic attack is a good approximation for the structure of the rate-limiting transition state. At any rate, the proposal of a single catalytic metal is supported by site-directed mutagenesis of metal ion-coordinating residues in BamHI. The inactive E113K mutant repels metal ion A, while the E77K mutant likely prevents metal ion B binding and exhibits reduced activity (*52*).

What is the advantage of having two ions instead of one at the active site while in other cases only one can be observed? This type of alternative way of achieving efficient catalysis with either two fixed or one mobile metal ion was first described by computational studies on DNA polymerase I (*44*). According to those results and our results presented here, the two metal ions have not only separate tasks but also different contributions to the catalytic effect.

A related scenario was observed in the case of RNaseH, where cocrystal structures of this nonspecific endonuclease from HIV-1 reverse transcriptase indicated the presence of two divalent metal ions at the active site (*53*), while in a related enzyme from *Escherichia coli*, only a single site was detected (*54*). On the basis of this discrepancy, an activation−attenuation model has been put forward, according to which the first metal ion activates while the second inhibits the reaction, fulfilling a regulatory role (*55*). Recent crystallographic analysis of RNaseH in complex with a RNA−DNA hybrid is compatible with a two-metal ion scheme and argues against such an activation−attenuation model (*56*).

In PD..D/ExK restriction endonucleases, where present, a regulatory function is suggested for the second metal ion based on our previous (*30*) and current results. Since this metal ion is more mobile than the one bound to the nucleophile, it can induce conformational rearrangements at the active site. Alternatively, it may modulate the pK_a of the water molecule that protonates the leaving group and thereby affect the energetics of the departure of the leaving group. The presence of the second metal ion might also switch between general base and *extrinsic* mechanisms for nucleophile generation.

In conclusion, on the basis of our results and accompanying biochemical and structural data, we propose the following catalytic scheme for BamHI action. The nucleophile is recruited from bulk solution and stabilized by metal ion A. The hydroxide ion remains bound to the metal ion during the nucleophilic attack. Thus, metal A not only plays a crucial role in the generation of the nucleophile but also is an important factor in the nucleophilic step. On the basis of the catalytic effect of the enzyme on the two reaction steps affecting the overall rate, BamHI optimizes the nucleophile preparation step more than the nucleophilic attack. Although the architecture of the active site is compatible with the two-metal ion mechanism, on the basis of the individual contribution of the metal ions, we propose that one metal ion is essential while the other is auxiliary for catalysis. Such a mechanistic scheme could be applicable to other restriction enzymes and thus could serve as a framework for a general mechanism for this enzyme family.

REFERENCES

1. Kovall, R. A., and Matthews, B. W. (1998) Structural, functional, and evolutionary relationships between λ-exonuclease and the type II restriction endonucleases, *Proc. Natl. Acad. Sci. U.S.A. 95*, 7893−7897.

2. Ban, C., and Yang, W. (1998) Structural basis for MutH activation in *E. coli* mismatch repair and relationship of MutH to restriction endonucleases, *EMBO J. 17*, 1526−1534.

3. Tsutakawa, S. E., Muto, T., Kawate, T., Jingami, H., Kunishima, N., Ariyoshi, M., Kohda, D., Nakagawa, M., and Morikawa, K. (1999) Crystallographic and functional studies of very short patch repair endonuclease, *Mol. Cell 3*, 621−628.

4. Kennedy, A. K., Haniford, D. B., and Mizuuchi, K. (2000) Single active site catalysis of the successive phosphoryl transfer steps by DNA transposases: Insights from phosphorothioate stereoselectivity, *Cell 101*, 295−305.

5. Hickman, A. B., Li, Y., Mathew, S. V., May, E. W., Craig, N. L., and Dyda, F. (2000) Unexpected structural diversity in DNA recombination: The restriction endonuclease connection, *Mol. Cell 5*, 1025−1034.

6. Chevalier, B. S., and Stoddard, B. L. (2001) Homing endonucleases: Structural and functional insight into the catalysts of intron/intein mobility, *Nucleic Acids Res. 29*, 3757−3774.

7. Beese, L. S., Friedman, J. M., and Steitz, T. A. (1993) Crystal structures of the Klenow fragment of DNA polymerase I complexed with deoxynucleoside triphosphate and pyrophosphate, *Biochemistry 32*, 14095−14101.

8. Steitz, T. A., and Steitz, J. A. (1993) A general two-metal-ion mechanism for catalytic RNA, *Proc. Natl. Acad. Sci. U.S.A. 90*, 6498−6502.

9. Bickle, T. A., and Kruger, D. H. (1993) Biology of DNA restriction, *Microbiol. Rev. 57*, 434−450.

10. Roberts, R. J., and Halford, S. E. (1993) in *Nucleases* (Linn, S. M., Lloyd, R. S., and Roberts, R. J., Eds.) pp 35−88, Cold Spring Harbor Laboratory Press, Plainview, NY.

11. Hiller, D. A., Fogg, J. M., Martin, A. M., Beechem, J. M., Reich, N. O., and Perona, J. J. (2003) Simultaneous DNA binding and bending by EcoRV endonuclease observed by real-time fluorescence, *Biochemistry 42*, 14375−14385.

12. Vipond, I. B., Baldwin, G. S., and Halford, S. E. (1995) Divalent metal ions at the active sites of the EcoRV and EcoRI restriction endonucleases, *Biochemistry 34*, 697−704.

13. Lagunavicius, A., Sasnauskas, G., Halford, S. E., and Siksnys, V. (2003) The metal-independent type IIs restriction enzyme BfiI is a dimer that binds two DNA sites but has only one catalytic centre, *J. Mol. Biol. 326*, 1051−1064.

14. Grazulis, S., Manakova, E., Roessle, M., Bochtler, M., Tamulaitiene, G., Huber, R., and Siksnys, V. (2005) Structure of the metal-independent restriction enzyme BfiI reveals fusion of a specific DNA-binding domain with a nonspecific nuclease, *Proc. Natl. Acad. Sci. U.S.A. 102*, 15797−15802.

15. Viadiu, H., and Aggarwal, A. K. (1998) The role of metals in catalysis by the restriction endonuclease BamHI, *Nat. Struct. Biol. 5*, 910−916.

16. Mordasini, T., Curioni, A., and Andreoni, W. (2003) Why do divalent metal ions either promote or inhibit enzymatic reactions? The case of BamHI restriction endonuclease from combined quantum-classical simulations, *J. Biol. Chem. 278*, 4381−4384.

17. Pingoud, A., Fuxreiter, M., Pingoud, V., and Wende, W. (2005) Type II restriction endonucleases: Structure and mechanism, *Cell. Mol. Life Sci. 62*, 685−707.

18. Horton, N. C., and Perona, J. J. (2004) DNA cleavage by EcoRV endonuclease: Two metal ions in three metal ion binding sites, *Biochemistry 43*, 6841−6857.

19. Etzkorn, C., and Horton, N. C. (2004) Mechanistic insights from the structures of HincII bound to cognate DNA cleaved from addition of Mg^{2+} and Mn^{2+}, *J. Mol. Biol. 343*, 833−849.

20. Jeltsch, A., Alves, J., Wolfes, H., Maass, G., and Pingoud, A. (1993) Substrate-assisted catalysis in the cleavage of DNA by the EcoRI and EcoRV restriction enzymes, *Proc. Natl. Acad. Sci. U.S.A. 90*, 8499−8503.

21. Grigorescu, A., Horvath, M., Wilkosz, P. A., Chandrasekhar, K., and Rosenberg, J. M. (2004) in *Restriction Endonucleases* (Pingoud, A., Ed.) pp 137−177, Springer, Berlin.

22. Lukacs, C. M., Kucera, R., Schildkraut, I., and Aggarwal, A. K. (2000) Understanding the immutability of restriction enzymes: Crystal structure of BglII and its DNA substrate at 1.5 Å resolution, *Nat. Struct. Biol. 7*, 134−140.

23. Kurpiewski, M. R., Engler, L. E., Wozniak, L. A., Kobylanska, A., Koziolkiewicz, M., Stec, W. J., and Jen-Jacobson, L. (2004) Mechanism of coupling between DNA recognition specificity and catalysis in EcoRI endonuclease, *Structure 12*, 1−20.

24. Jeltsch, A., Pleckaityte, M., Selent, U., Wolfes, H., Siksnys, V., and Pingoud, A. (1995) Evidence for substrate-assisted catalysis in the DNA cleavage of several restriction endonucleases, *Gene 157*, 157−162.

25. Horton, N. C., Newberry, K. J., and Perona, J. J. (1998) Metal ion-mediated substrate-assisted catalysis in type II restriction endonucleases, *Proc. Natl. Acad. Sci. U.S.A. 95*, 13489−13494.

26. Horton, N. C., Otey, C., Lusetti, S., Sam, M. D., Kohn, J., Martin, A. M., Ananthnarayan, V., and Perona, J. J. (2002) Electrostatic contributions to site specific DNA cleavage by EcoRV endonuclease, *Biochemistry 41*, 10754−10763.

27. Horton, N. C., and Perona, J. J. (2000) Crystallographic snapshots along a protein-induced DNA-bending pathway, *Proc. Natl. Acad. Sci. U.S.A. 97*, 5729−5734.

28. Newman, M., Strzelecka, T., Dorner, L. F., Schildkraut, I., and Aggarwal, A. K. (1994) Structure of restriction endonuclease BamHI and its relationship to EcoRI, *Nature 368*, 660−664.

29. Newman, M., Strzelecka, T., Dorner, L. F., Schildkraut, I., and Aggarwal, A. K. (1995) Structure of Bam HI endonuclease bound to DNA: Partial folding and unfolding on DNA binding, *Science 269*, 656−663.

30. Mones, L., Simon, I., and Fuxreiter, M. (2007) Metal-binding sites at the active site of restriction endonuclease BamHI can conform to a one-ion mechanism, *Biol. Chem. 388*, 73−78.

31. Warshel, A., and Weiss, R. M. (1980) An empirical valence bond approach for comparing reactions in solutions and in enzymes, *J. Am. Chem. Soc. 102*, 6218−6226.

32. Warshel, A., Sharma, P. K., Kato, M., Xiang, Y., Liu, H., and Olsson, M. H. (2006) Electrostatic basis for enzyme catalysis, *Chem. Rev. 106*, 3210−3235.

33. Warshel, A. (1991) *Computer modeling of chemical reactions in enzymes and solutions*, John Wiley & Sons, New York.

34. Warshel, A., and Florian, J. (2004) in *The Encyclopedia of Computational Chemistry* (Schleyer, P. v. R., Jorgensen, W. L., Schaefer, H. F., III, Schreiner, P. R., Thiel, W., and Glen, R., Eds.) John Wiley & Sons, Chichester, U.K.

35. Case, D. A., Darden, T. A., Cheatham, T. E., III, Simmerling, C. L., Wang, J., Duke, R. E., Luo, R., Merz, K. M., Wang, B., Pearlman, D. A., Crowley, M., Brozell, S., Tsui, V., Gohlke, H., Mongan, J., Hornak, V., Cui, G., Beroza, P., Schafmeister, C., Caldwell, J. W., Ross, W. S., and Kollman, P. A. (2004) *Amber 8*, University of California, San Francisco.

36. Florian, J., Goodman, M. F., and Warshel, A. (2003) Computer simulation of the chemical catalysis of DNA polymerases: Discriminating between alternative nucleotide insertion mechanisms for T7 DNA polymerase, *J. Am. Chem. Soc. 125*, 8163−8177.

37. Marelius, J., Kolmodin, K., Feierberg, I., and Åqvist, J. (1998) Q: A molecular dynamics program for free energy calculations and empirical valence bond simulations in biomolecular systems, *J. Mol. Graphics Modell. 16*, 213−225.

38. Cornell, W. D., Cieplak, R., Bayly, C. L., Gould, I. R., Merz, K. M., Ferguson, D. M., Spellmeyer, D. G., Fox, T., Caldwell, J. W., and Kollman, P. A. (1995) A second generatin force field for the simulation of proteins, nucleic acids, and organic molecules, *J. Am. Chem. Soc. 117*, 5179−5197.

39. Eigen, M., and de Mayer, L. (1955) Kinetics of neutralization, *Z. Electrochem. 59*, 986−993.

40. Åqvist, J., and Warshel, A. (1989) Calculations of free energy profiles for the staphylococcal nuclease catalyzed reaction, *Biochemistry 28*, 4680−4689.

41. Cabani, S., Gianni, P., Mollica, V., and Lepori, L. (1981) Group contributions to the thermodynamic properties of non-ionic organic solutes in dilute aqueous solution, *J. Solution Chem. 10*, 563−595.

42. Florian, J., and Warshel, A. (1997) Langevin Dipoles Model for Ab Initio Calculations of Chemical Processes in Solution: Parametrization and Application to Hydration Free Energies of Neutral and Ionic Solutes and Conformational Analysis in Aqueous Solution, *J. Phys. Chem. B 101*, 5583−5595.

43. Warshel, A. (1981) Calculations of enzymatic reactions: Calculations of pK_a, proton transfer reactions, and general acid catalysis reactions in enzymes, *Biochemistry 20*, 3167−3177.

44. Fothergill, M., Goodman, M. F., Petruska, J., and Warshel, A. (1995) Structure-energy analysis of the role of metal ions in phosphodiester bond hydrolysis by DNA polymerase I, *J. Am. Chem. Soc. 117*, 11619−11627.

45. Borden, J., Crans, D. C., and Florian, J. (2006) Transition state analogues for nucleotidyl transfer reactions: Structure and stability of pentavalent vanadate and phosphate ester dianions, *J. Phys. Chem. B 110*, 14988−14999.

46. Guthrie, J. P. (1977) Hydration and Dehydration of Phosphoric Acid Derivatives: Free Energies of Formation of the Pentacoordinate Intermediates for Phosphate Ester Hydrolysis and Monomeric Metaphosphate, *J. Am. Chem. Soc. 99*, 3991−4000.

47. Engler, L. E., Sapienza, P., Dorner, L. F., Kucera, R., Schildkraut, I., and Jen-Jacobson, L. (2001) The energetics of the interaction of BamHI endonuclease with its recognition site GGATCC, *J. Mol. Biol. 307*, 619−636.

48. Fuxreiter, M., and Osman, R. (2001) Probing the general base catalysis in the first step of BamHI action by computer simulations, *Biochemistry 40*, 15017−15023.

49. Bren, U., Martinek, V., and Florian, J. (2006) Decomposition of the solvation free energies of deoxyribonucleoside triphosphates using the free energy perturbation method, *J. Phys. Chem. B 110*, 12782−12788.

50. Mark, A. E., and van Gunsteren, W. F. (1994) Decomposition of the free energy of a system in terms of specific interactions. Implications for theoretical and experimental studies, *J. Mol. Biol. 240*, 167−176.

51. Shen, Y., Zhukovskaya, N. L., Guo, Q., Florian, J., and Tang, W. J. (2005) Calcium-independent calmodulin binding and two-metal-ion catalytic mechanism of anthrax edema factor, *EMBO J. 24*, 929−941.

52. Viadiu, H. (1999) Structural study of specificity and catalysis by restriction endonuclease BamHI, Ph.D. Dissertation, p 92, Columbia University, New York.

53. Davies, J. F., II, Hostomska, Z., Hostomsky, Z., Jordan, S. R., and Matthews, D. A. (1991) Crystal structure of the ribonuclease H domain of HIV-1 reverse transcriptase, *Science 252*, 88−95.

54. Katayanagi, K., Okumura, M., and Morikawa, K. (1993) Crystal structure of *Escherichia coli* RNase HI in complex with Mg^{2+} at 2.8 Å resolution: Proof for a single Mg^{2+}-binding site, *Proteins 17*, 337−346.

55. Keck, J. L., Goedken, E. R., and Marqusee, S. (1998) Activation/attenuation model for RNase H. A one-metal mechanism with second-metal inhibition, *J. Biol. Chem. 273*, 34128−34133.

56. Nowotny, M., Gaidamakov, S. A., Crouch, R. J., and Yang, W. (2005) Crystal structures of RNase H bound to an RNA/DNA hybrid: Substrate specificity and metal-dependent catalysis, *Cell 121*, 1005−1016.